

Synthesis, structure and spectroscopic properties of luminescent $\text{GdVO}_4:\text{Dy}^{3+}$ and DyVO_4 particles



Dragana J. Jovanović ^{a,*}, Andrea Chiappini ^{b,**}, Lidia Zur ^{e,b}, Tamara V. Gavrilović ^{a,g}, Thi Ngoc Lam Tran ^{c,b,d}, Alessandro Chiasera ^b, Anna Lukowiak ^f, Krisjanis Smits ^g, Miroslav D. Dramićanin ^a, Maurizio Ferrari ^{b,e}

^a Vinča Institute of Nuclear Sciences, University of Belgrade, P.O. Box 522, 11001 Belgrade, Serbia

^b IFN-CNR CSMFO Lab. and FBK Photonics Unit, Via alla Cascata 56/C, 38123 Povo-Trento, Italy

^c Department of Civil, Environmental and Mechanical Engineering, Trento University, Via Mesiano, 77, 38123 Trento, Italy

^d Ho Chi Minh City University of Technical Education, 1 Vo Van Ngan Street, Thu Duc District, Ho Chi Minh City, Viet Nam

^e Enrico Fermi Center, Piazza del Viminale 1, 00184 Roma, Italy

^f Institute of Low Temperature and Structure Research, Polish Academy of Sciences, 2 Okolna St., 50-422 Wrocław, Poland

^g Institute of Solid State Physics, University of Latvia, 8 Kengaraga Street, Riga, LV-1063, Latvia

ARTICLE INFO

Article history:

Received 15 December 2017

Received in revised form

22 December 2017

Accepted 25 December 2017

ABSTRACT

In this work, we focused on the syntheses, structure and spectroscopic properties of $\text{GdVO}_4:\text{Dy}^{3+}$ and DyVO_4 (nano)particles of different sizes and shapes (spherical nanoparticles of 2 nm, 4 nm, and 20 nm in size, nanorods with a few nanometers in diameter and up to 10–20 nm in length and microparticles of 1–8 μm) obtained by four synthetic methods. The size effect on the structure, Raman active modes, and photoluminescence emission intensities was analyzed by X-ray diffraction, Raman and photoluminescence spectroscopy, scanning and transmission electron microscopy, and diffuse reflection spectroscopy. All X-ray diffraction patterns clearly indicated presence of a single tetragonal zircon-type phase; absence of impurity phases indicate that the dopant Dy^{3+} ions were successfully and uniformly incorporated into the GdVO_4 host lattice due to the equal valence and similar ionic radii. Micro-Raman measurements support the XRD measurements and showed Raman-active modes of the REVO₄ systems (RE = Gd, Dy). The difference between the two hosts in the diffuse reflectance spectra was observed and it could be attributed to more effective Gd^{3+} ions on the charge transfer bands and different polarization (compared to bulk material) in smaller nanoparticles. Photoluminescence spectroscopy showed several bands in the visible and near-infrared regions which can be exclusively attributed to the f-f transitions of Dy^{3+} ions.

© 2017 Elsevier B.V. All rights reserved.

1. Introduction

Lanthanide (Ln)-doped luminescent inorganic materials play an important role in everyday life due to their unique structural and physicochemical properties, in particular, optical properties which make them potentially useful in a wide range of applications. These materials, both microcrystalline and nanocrystalline, can exhibit down-conversion or up-conversion luminescence under ultraviolet (UV) or near-infrared (NIR) excitation, depending on the selected

dopant ions and crystal structure of the host material. Ln-doped phosphors are primarily used in conventional, novel, and emerging display and lighting technologies and their advantages include high energy conversion efficiency, purity in spectral colors, strong emission and high thermal stability and conductivity [1–4].

Rare-earth orthovanadates with general formula REVO₄ (where RE is a rare-earth element, including lanthanoids from La to Lu as well as Y and Sc) have proved to be good host lattices for optically-active trivalent Ln ions. Due to the same valence, similar ionic radii, electronegativities and electronic structures between RE ions in a host and dopant ions, doping is possible in a wide range of concentrations without much affecting the lattice structure. Such materials exhibit intense luminescence emission caused by an efficient energy transfer from the vanadate groups to Ln ions, and

* Corresponding author.

** Corresponding author.

E-mail addresses: draganj@vinca.rs (D.J. Jovanović), [\(A. Chiappini\).](mailto:chiappini@fbk.eu)

wide colour tuning is easily made by selection of dopant ions. Both undoped and Ln-doped REVO₄ nanostructures have been extensively studied as an important class of multifunctional materials which are very attractive for different applications such as phosphors, optical polarizers, laser host materials, scintillators, and photocatalysts [5–8].

By appropriate selection of a matrix, Dy³⁺-doped materials show excellent luminescent properties due to a large number of closely spaced energy levels in the visible (Vis), NIR and mid-infrared (Mid-IR) spectral regions. In the Vis region, Dy³⁺ generally have two dominant emission bands. One is the blue band due to the ${}^4F_{9/2} \rightarrow {}^6H_{15/2}$ transition, while another is the yellowish band due to the hypersensitive ${}^4F_{9/2} \rightarrow {}^6H_{13/2}$ transition. Since Dy³⁺ ions are among several the NIR and Mid-IR emitting Ln ions, Dy³⁺-based materials have been studied as potentially useful in the NIR and Mid-IR region, in particular, in construction of Mid-IR lasers and amplifiers [9,10].

It is well known that all physical, chemical, mechanical and optical properties are size-dependent in nano-scale range. The nanomaterials generally are showing reduced quantum efficiency of emission in small-size particles. Up to now, the size effect on photoluminescent properties of several different materials has been studied [11–13].

Herein, our focus was mainly on the syntheses, structure and spectroscopic properties of luminescent GdVO₄:Dy³⁺ and DyVO₄ (nano)particles of different sizes and shapes. In particular, with a view to incorporating Dy³⁺-containing nanoparticles in silica waveguides, it was interesting to assess their luminescence performance in the NIR region. GdVO₄ was used as a host for Dy³⁺ ions because of several reasons: an easy doping, high absorption cross section, low phonon energy, efficient energy transfer from VO₄³⁻ group to the Dy³⁺ ions, low sensitivity to humidity, high melting point (~1800 °C), and high potential for multi-functional applications [7,8]. Unlike GdVO₄, DyVO₄ is relatively less studied and only dozen or so reports on it are available in the recent literature [14].

2. Experimental

2.1. Materials and methods

Two different series of powdered samples, S1 and S2, respectively, of GdVO₄:Dy³⁺ and DyVO₄ with different particle sizes were synthesized by four different methods: the high-temperature solid-state, co-precipitation, reverse micelle and colloidal techniques. All chemicals: gadolinium(III) oxide, Gd₂O₃ (99.99%, Alfa Aesar), dysprosium (III) oxide, Dy₂O₃ (99.99%, Alfa Aesar), gadolinium (III) nitrate hexahydrate Gd(NO₃)₃ × 6H₂O (99.99%, Alfa Aesar), dysprosium (III) nitrate hexahydrate, Dy(NO₃)₃ × 6H₂O (99.9%, Alfa Aesar), ammonium vanadate, NH₄VO₃ (Alfa Aesar, 99.999%), Na₃C₆H₅O₇ × 2H₂O, trisodium citrate dihydrate (>99%, Sigma Aldrich), NaOH, cyclohexane, Triton X-100, and n-pentanol were of the highest purity commercially available and were used without further purification. Milli-Q deionized

water (electrical resistivity = 18.2 MΩ cm⁻¹) was used as a solvent.

Using different techniques of synthesis, the series S1 and S2 were prepared similarly to our previously reported syntheses of Ln-doped GdVO₄ materials [8,15–17]. Throughout the manuscript, the samples are denoted as in Table 1 (See below). For the GdVO₄:Dy³⁺ samples concentration of Dy³⁺ ions was 2 mol% with respect to Gd³⁺ ions. Here, procedures used for preparation of GdVO₄:Dy³⁺ are given in more detail, while the DyVO₄ samples were produced analogously.

2.1.1. The high-temperature solid-state method

In a typical synthesis, the Gd₂O₃, Dy₂O₃ and NH₄VO₃, were homogeneously mixed by dry grinding and heated for 1 h in open crucibles at 800 °C. The products were removed from the furnace, cooled down to room temperature, ground, and reheated at 1100 °C for 3 h to complete the reaction. Then, the powder was homogeneously ground, washed with 2 M NaOH solution water and methanol and finally calcined at 1150 °C for 90 min to improve the crystallinity of material and to remove ligands attached to particle surfaces during the washing step.

2.1.2. The co-precipitation method

Typically, an appropriate amount of NH₄VO₃ was dissolved in aqueous solutions of NaOH. A mixture of aqueous solutions of Gd³⁺ and Dy³⁺ ions was added drop-wise to a NH₄VO₃ solution. A formed milk-white opalescent precipitate of GdVO₄:Dy³⁺ was additionally heated and stirred at 70 °C for 1 h. The precipitate was separated from the suspension by centrifugation, and washed several times with distilled water. Finally, the collected powder of GdVO₄:Dy³⁺ was dried at 70 °C in the air for 20 h. To improve their crystallinity and to get particles of different size and morphology, the as-prepared powder was additionally annealed at 600 °C for 2 h.

2.1.3. Reverse micelles method

A typical synthesis was performed at room temperature by using three separately prepared solutions: 1) An oil phase mixture of cyclohexane, Triton X-100, and n-pentanol in a corresponding volume ratio; 2) a mixture of aqueous solutions of Gd(NO₃)₃ × 6H₂O and Dy(NO₃)₃ × 6H₂O and, 3) an aqueous solution of NH₄VO₃. The solution 3) was drop-wise added into mixture of the solutions 1) and 2) under continuous magnetic stirring. After stirring and aging for 24 h, methanol was added to destabilize the solution and resulting precipitate was separated by centrifugation and washed several times by methanol and water. The collected precipitate of GdVO₄:Dy³⁺ was dried at 70 °C in the air for 20 h.

2.1.4. Colloidal synthesis

It is noteworthy that, to the best of our knowledge, both, GdVO₄:Dy and DyVO₄ nanoparticles were obtained, for the first time, in the colloidal form with the lowest diameter ever reported. In brief, solution of trisodium citrate dihydrate was added drop by drop to the mixture of Gd(NO₃)₃ × 6H₂O and Dy(NO₃)₃ × 6H₂O solution,

Table 1

Sample names, method of synthesis, preparation temperature and obtained morphology and size.

Samples name	Method of synthesis	Preparation temperature T (°C)	Morphology and size
S1-1 (GdVO ₄ :Dy)	High-temperature solid-state	1150	Irregular spheres 1–8 μm
S2-1 (DyVO ₄)			Nanospheres 20 nm
S1-2 (GdVO ₄ :Dy)	Co-precipitation with annealing	600	Nanorods 2 nm × 10 nm
S2-2(DyVO ₄)			Nanospheres 4 nm
S1-3 (GdVO ₄ :Dy)	Co-precipitation without annealing	70	Nanospheres Nanorods
S2-3 (DyVO ₄)			Nanospheres 2 nm
S1-4 (GdVO ₄ :Dy)	Reverse micelle	70	Nanospheres Nanorods
S2-4 (DyVO ₄)			Nanospheres 4 nm
S1-5 (GdVO ₄ :Dy)	Colloidal	70	Nanospheres Nanorods
S2-5 (DyVO ₄)			2 nm

followed by vigorous stirring at room temperature. After complexation between Gd^{3+} (Dy^{3+}) and citrate ions, the solution of NH_4VO_3 was added. The slow growth of particles and the removal of excess ions were achieved by dialysis against distilled water for 24 h. Powder samples were finally obtained upon evaporating the aqueous colloidal solutions and drying them in the air at 70 °C for 20 h.

2.2. Characterization methods and instrumentation

Powder X-ray diffraction (XRD) measurements were performed on a Rigaku SmartLab diffractometer using $\text{Cu-K}_{\alpha 1,2}$ radiation ($\lambda = 0.15405 \text{ nm}$). Diffraction data were recorded with a step size of 0.01° and a counting time of 1 deg/min over the 2θ range of 10°–90°. Transmission electron microscopy (TEM) studies were made on a Tecna G20 (FEI) operated at an accelerating voltage of 200 kV with point resolution of 0.25 nm and line resolution 0.102 nm. Microstructural characterization was done using a JEOL JSM-6610LV scanning electron microscope (SEM). Diffuse reflection spectra measurements were recorded with 1 nm resolution on a Shimadzu UV–Visible UV-2600 (Shimadzu Corporation, Japan) spectrophotometer equipped with an integrated sphere (ISR-2600 Plus (for UV-2600)) in the range from 220 nm to 1350 nm. Luminescence measurements in UV–Vis region were performed with an Fluorolog-3 Model FL3-221 spectrofluorometric system (Horiba JobinYvon) utilizing a 450 W Xenon lamp as an excitation source for steady-state emission measurements. μ Raman spectra were recorded using a Labram Aramis Jobin Yvon Horiba μ Raman system with a He-Ne laser source of 632 nm and equipped with a confocal microscope and an air-cooled CCD. A 100X objective was used to focus the laser on the sample as well as to collect the Raman spectra, with a spatial resolution of about 1 μm . A wave-number accuracy of about 2 cm^{-1} can be achieved with an 1800 line/mm grating. Photoluminescent (PL) spectroscopy of Dy^{3+} ions transitions in the NIR region was performed using the 488 nm line of an Ar^+ ion laser as an excitation source and 330 nm of a Xenon lamp. The luminescence was dispersed by a 320 mm single-grating monochromator with a resolution of 1 nm. The light was detected using a Hamamatsu photomultiplier tube and standard lock-in technique. Excitation spectra were recorded using a Xe lamp coupled to a single grating monochromator as an excitation source, in a spectral range extending from 250 to 650 nm. Finally, quantum yield measurements have been obtained by Hamamatsu Quantaurus-QY C11347-11.

3. Results and discussions

3.1. Structural and microstructural properties

(Bulk) samples obtained by the high-temperature solid-state method were studied in detail by SEM, while all other (nanostructured) samples were examined by TEM. No difference in morphologies between the two series of samples (see Table 1) was observed and the only representative SEM/TEM images for $\text{GdVO}_4:\text{Dy}^{3+}$ at two different resolutions (photographs at left and right) are presented in Fig. 1. The SEM images (Fig. 1a and b) show that the powders are composed of chunks of irregular spherical particles with an average diameter ranging from 1 μm to 8 μm . Nanoparticles (about 20 nm in size) could be seen in the TEM micrographs (Fig. 1c and d) of the powders prepared by co-precipitation method and annealed at 600 °C.

As is shown for $\text{GdVO}_4:\text{Dy}^{3+}$ (Fig. 1e and f), the powders of non-annealed as-prepared $\text{GdVO}_4:\text{Dy}^{3+}$ and DyVO_4 obtained by co-precipitation are self-organized in nanorods bunches that are oriented to each other in range of different angles. The bundles contain 5–6 nanorods with diameter size of 2–3 nm and about 10 nm in length. High-magnification TEM images (Fig. 1g and h) show nanoparticles approximately 3–4 nm in diameter obtained

for samples fabricated by reverse micelle method. This finding is consistent with the crystallite size evaluated by means the XRD measurements. Note that similar values for the crystalline domain size and the microscopically estimated average particle size of the nanoparticles imply that each particle consists of a single crystallite. The smallest nanoparticles, nanospheres of about 2 nm in size (see Fig. 1i and j), were produced by colloidal route.

Typical XRD patterns of all prepared powders are shown in Fig. 2. All the patterns clearly indicate the presence of a single tetragonal zircon-type phase of GdVO_4 (DyVO_4) matching closely with JCPDS card No. 00-017-0260, and JCPDS card No. 00-016-0870, respectively. Both, GdVO_4 and DyVO_4 , crystallize in the zircon-type (ZrSiO_4) structure ($Z = 4$, space group $I4_1/\text{amd}$) at ambient conditions. In this structure the vanadium atom in the $[\text{VO}_4]^{3-}$ groups is tetrahedrally coordinated with O^{2-} ions, while the Gd^{3+} or Dy^{3+} cations are coordinated by eight oxygen atoms forming a distorted dodecahedron [18].

The absence of impurity phases and very small shift of reflections compared to the reflection positions of pure GdVO_4 indicate that the dopant Dy^{3+} ions were successfully and uniformly incorporated into the GdVO_4 host lattice due to the equal valence (+3) and similar ionic radii (Dy^{3+} , ionic radius = 1.027 Å and Gd^{3+} , ionic radius = 1.053 Å). Relatively intensive and narrow reflection peaks suggest that samples synthesized at higher temperature are highly crystalline, and that no additional thermal treatment is necessary. However, the XRD diffraction patterns of thermally untreated samples indicate the presence of an amorphous phase.

All structural parameters (average crystal size, unit cell parameters and strain) of the synthesized $\text{GdVO}_4:\text{Dy}^{3+}$ and DyVO_4 particles with different sizes were estimated by the Halder-Wagner method and by structural Rietveld refinement and these values are given in Table 2. There is a significant difference in the lattice volume (See Fig. 3) between bulk particles and nanoparticles. It has been noted that the size of the unit cell is larger in small nanoparticles (S1-5 and S2-5) made up of small crystals than unit cell for micrometer samples (S1-1 and S2-1). Nanorods are an exception (Fig. 3) maybe due to different morphology and orientation of nanoparticles. The lattice expansion could be related to several effects on particle surface, such as: defects, cation auto-reduction, absorbed molecules and negative surface stress [18,19].

Micro-Raman measurements support the XRD measurements and the observed Raman active modes are in a good agreement with the data in the literature. As discussed in Ref. [20], the Raman-active modes of the REVO_4 system, which can be considered to be composed of two sublattices of RE and VO_4 units, are decomposed in the terms of the irreducible representations of the D_{4h} point group as:

$$\Gamma = A_{1g}(v_1, v_2) + B_{1g}(2T, v_3, v_4) + B_{2g}(v_2) + E_g(2T, R, v_3, v_4) \quad (1)$$

where v_i ($i = 1, \dots, 4$) correspond to four internal vibrational modes (symmetric and asymmetric stretching and bending) of the VO_4 tetrahedron and T/R corresponds, respectively, to the translational or rotational motion involving both the RE and VO_4 units [21].

Analyzing the Raman spectra reported in Fig. 4, we can clearly see the Raman-active modes of the REVO_4 systems (RE = Gd, Dy): the modes observed in the region 260–1000 cm^{-1} are internal stretching and bending vibrations of the VO_4 tetrahedra and the modes observed at 124, 156, and 245 cm^{-1} are external ones.

The difference in the Raman position for the bulk particles of two series, can be attributed to the difference in atomic numbers between Dy and Gd [21]. Focusing the attention on the samples with low dimensions we can observe differences related to the broadening and the shift of the Raman peaks that could be attributed to inhomogeneous distributions and different polarization in smaller nanoparticles compared to bulk material [22].

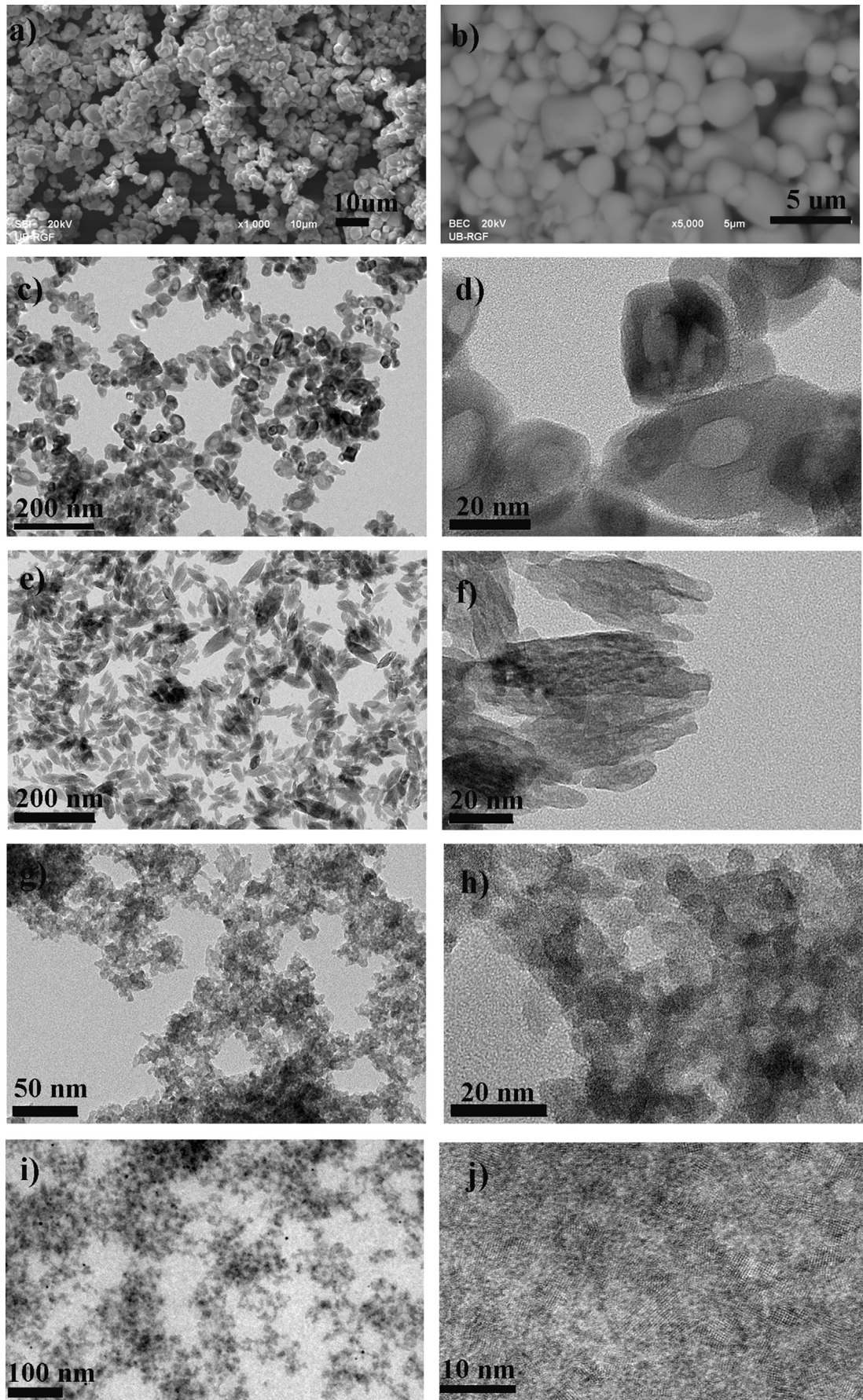


Fig. 1. SEM/TEM images at two different resolutions (left and right) of (nano)particles prepared by different synthetic methods: the solid state method (a,b); co-precipitation with annealing at $T = 600\text{ }^{\circ}\text{C}$ (c,d); co-precipitation without annealing (e,f); reverse micelle method (g,h); colloidal route (i,j).

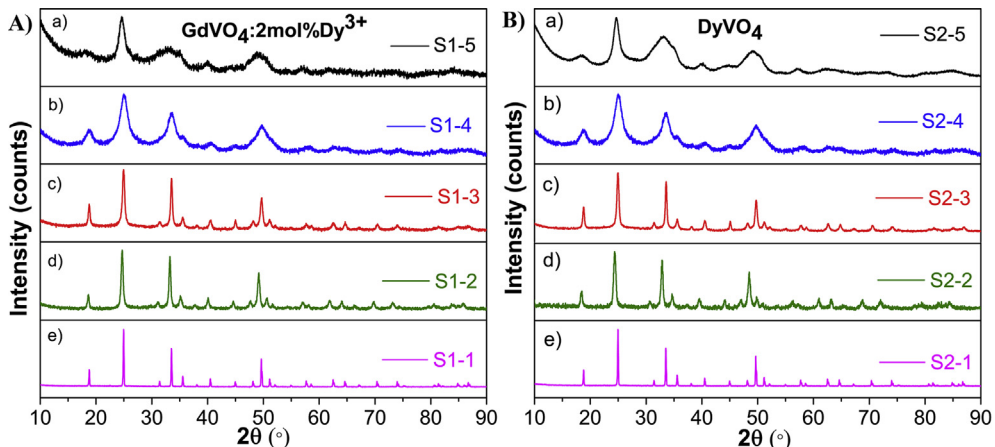


Fig. 2. XRD patterns for: A) Series I (GdVO₄:Dy³⁺) and B) Series II (DyVO₄) (nano)particles of different sizes: a) 2 nm; b) 4 nm; c) nanorods 2 nm × 10 nm; d) 20 nm and e) 1–8 μm (bulk material).

Table 2

Structural parameters of the synthesized GdVO₄:Dy³⁺ and DyVO₄ particles of different sizes.

Samples	Average crystal size (nm)	Unit cell parameters			
		a = b (Å)	c (Å)	V (Å) ³	strain
S1-1	56.0	7.149	6.307	322.34	0.077
S1-2	18.7	7.182	6.308	326.41	0.16
S1-3	13.8	7.147	6.303	321.96	0.13
S1-4	3.8	7.166	6.375	327.37	1.13
S1-5	1.9	7.287	6.315	335.33	1.70
S2-1	55.9	7.146	6.306	322.02	0.079
S2-2	18.2	7.186	6.303	325.48	0.28
S2-3	14.3	7.136	6.286	320.09	1.13
S2-4	4.1	7.149	6.390	326.58	0.75
S2-5	2.1	7.292	6.384	339.46	1.2

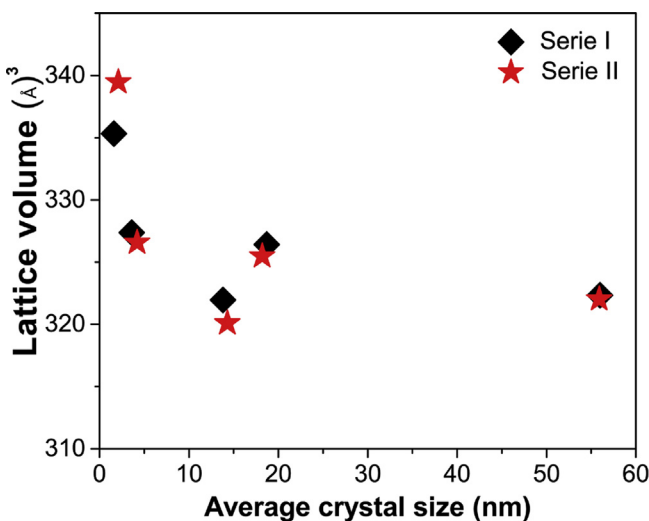


Fig. 3. Dependence of lattice volume on average crystal size.

3.2. Optical properties

3.2.1. Diffuse reflectance spectra

Diffuse reflectance spectra of the powdered samples from Series I (GdVO₄:Dy) and Series II (DyVO₄) in the UV–Vis–NIR range are

given in Fig. 5a and b. In the Vis–NIR region, the spectra exhibit similar spectral features: for both Series strong bands appear at the same wavelength positions (754 nm, 809 nm, 866 nm, 906 nm, 1105 nm and 1306 nm) and correspond respectively to intra-configurational 4f⁹–4f⁹ electron transitions from the ⁶H_{15/2} ground state to the ⁶F_{3/2} (⁶F_{1/2}), ⁶F_{5/2}, ⁶F_{7/2}, ⁶H_{5/2}, ⁶H_{7/2} (⁶F_{9/2}) and ⁶H_{9/2} (⁶F_{11/2}) excited states of the Dy³⁺ ions [23].

In the UV region, broad and strong bands of all the samples could be attributed to charge transfer (CT) transitions inside VO₄³⁻ groups. The (one-electron) charge transfer occurs between the 2p orbital of oxygen (O²⁻) and the vacant 3d orbital of the central vanadium (V⁵⁺) in the tetrahedral VO₄³⁻ with T_d symmetry. According to the molecular orbital theory, energy levels involved are the ground ¹A₁ state and the excited ¹T₁, ¹T₂, ³T₁, and ³T₂ states. Then, in all the vanadates, the transitions ¹A₁ → (¹T₁, ¹T₂) give rise to a broad and intense CT absorption band in the UV region [24].

However, as it can be seen from Fig. 5a and b, there is a difference between two series of samples. Although all the samples exhibit absorption in the same spectral region, it appears that Gd³⁺ ions more affect the CT bands. Regarding Series I (Fig. 5a), it seems that CT is more prominent for smaller nanoparticles (samples: S1-3, S1-4 and S1-5) than larger ones (sample S1-4) and bulk material (sample S1-5). Some other differences in the spectra could be attributed to different polarization (compared to bulk material) in smaller nanoparticles.

The band gap values calculated from the corresponding diffuse reflectance spectra are given in Table 3. The band gap, E_g, was estimated from the absorption edge wavelength of the inter-band transition according to the following equation:

$$(F_{KM}(R) \times E_{phot.})^2 = A(E_{phot.} - E_g), \quad (2)$$

where F_{KM}(R) is the Kubelka–Munk function, with $F_{KM}(R) = (1-R)^2/2R$, R is the observed reflectance, A is the constant, and E_{phot.} is the photon energy (hv). According to Equation (2), the corresponding band gap E_g value was determined by extrapolating the steepest portion of the graph on the E_{phot.} axis at $(F_{KM}(R) \times E_{phot.})^2 = 0$ (shown in Fig. 5c and d). The calculated band gap energies are given in Table 3.

Note that the increase in band gap values with a decrease in size of nanoparticles can hardly be attributed to a quantum confinement effect. The main reason is that the Bohr radii for vanadate hosts appear to be very small. For instance, for lanthanide-doped YVO₄ materials, Mialon calculated that Bohr radius is 1.15 Å [25]. However, the increase of band gap energies, could be related to the Moss–Burstein effect. This effect arises when the electron carrier

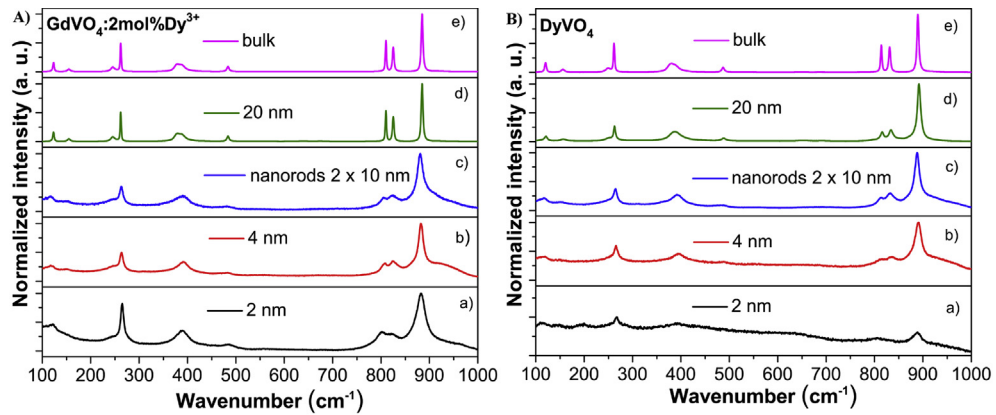


Fig. 4. Micro-Raman bands for: A) Series I ($\text{GdVO}_4:\text{Dy}^{3+}$) and B) Series II (DyVO_4) nanoparticles with size: a) 2 nm; b) 4 nm; c) nanorods 2 nm \times 10 nm; d) 20 nm and e) 1–8 μm (bulk material).

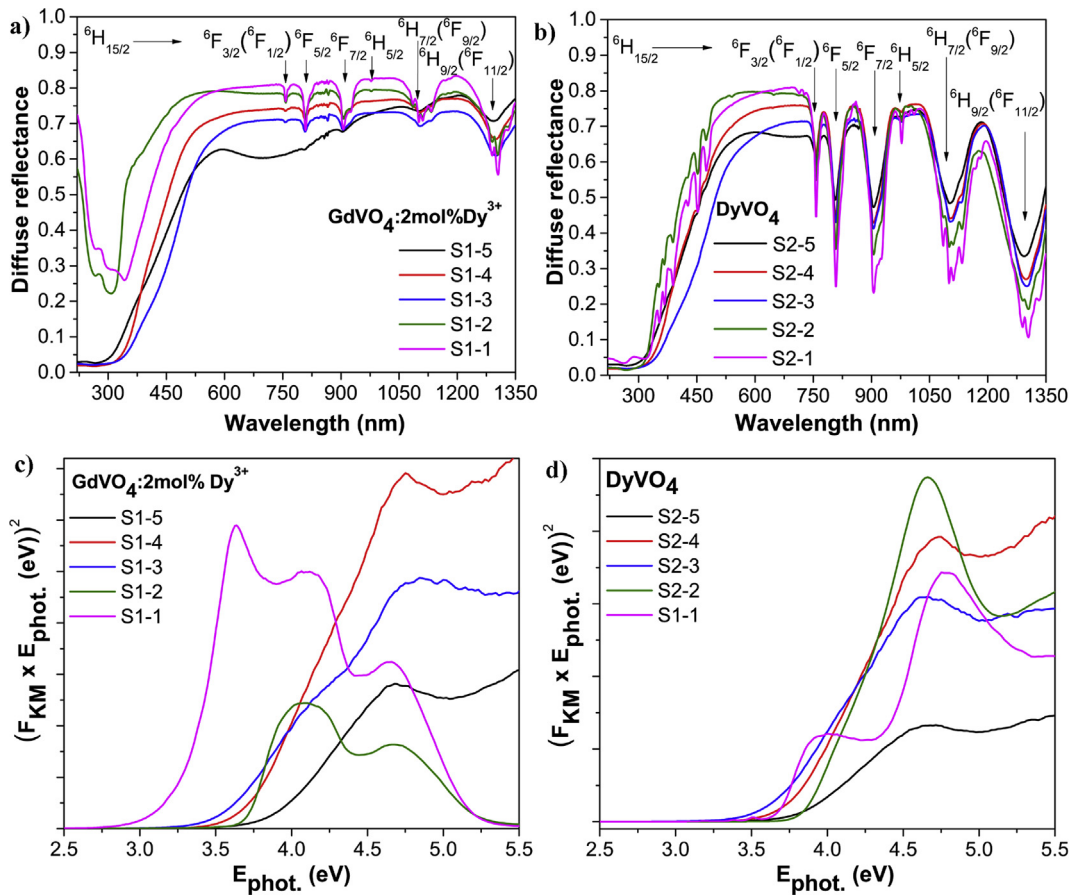


Fig. 5. Diffuse reflectance spectra for: a) Series S1 and b) Series S2; and the $(F_{KM}(R)E_{phot})^2$ vs. photon energy (Kubelka-Munk) plots of the samples for: c) Series I and d) Series II.

Table 3
Estimated band gap energy, E_g (eV), for all synthesized samples.

Samples	Band gap values E_g (eV)
S1-1	3.28
S2-1	3.65
S1-2	3.70
S2-2	3.86
S1-3	3.51
S2-3	3.65
S1-4	3.72
S2-4	3.78
S1-5	3.86
S2-5	3.79

concentration exceeds the conduction band edge density of states and the Fermi level, which now lies in the conduction band since all the states below the Fermi level are occupied states. In nanocrystalline materials band bending effect takes place at grain boundaries due to their increased surface to volume ratio. For smaller grains, the band bending effect is large where as it becomes flatter for larger grains [26].

3.2.2. Photoluminescence emission spectra in the UV–Vis spectral region

It is well-known that, under UV excitation, the vanadate materials themselves show luminescence emission originating from

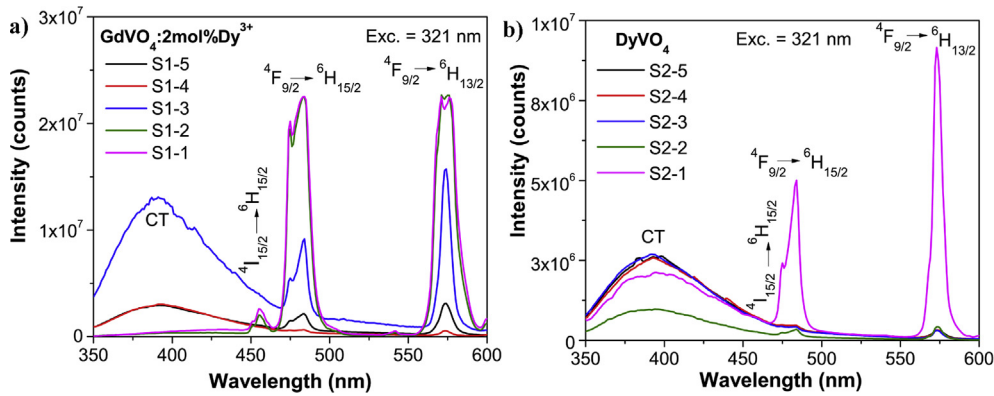


Fig. 6. Photoluminescence spectra for: a) Series S1 and b) Series S2 recorded (under excitation with 321 nm radiation) at room temperature.

transitions inside VO_4^{3-} groups. Moreover, GdVO_4 is an excellent host material for Ln ions such as Eu^{3+} , Dy^{3+} , Sm^{3+} , Tm^{3+} , etc. for two reasons: (a) following UV absorption, the excited vanadate groups VO_4^{3-} can effectively transfer energy to Ln dopant ions, thus exciting them to higher energy states and (b) Gd^{3+} has a strong absorption peak at ~280 nm and thereby energy transfer is possible to the excited states of the activators (Ln^{3+}) [27].

Fig. 6 shows photoluminescence (PL) emission spectra in the UV–Vis spectral region excited at 321 nm. In almost all samples, a host emission was observed as a broad band with tail up to 500 nm and maximum at about 370 nm. It could be recognized as symmetric part of CT attributed to the transitions ($^3\text{T}_1, ^3\text{T}_2$) $\rightarrow ^1\text{A}_1$ of the VO_4^{3-} groups. All the spectra show the Dy^{3+} ions emission from two closely separated states ($^4\text{F}_{9/2}$ and $^4\text{I}_{15/2}$) to the ground state ($^6\text{H}_{15/2}$), peaking at 483 and 455 nm, and from $^4\text{F}_{9/2}$ to the $^6\text{H}_{13/2}$ transition, peaking at 572 nm. Regarding Series 1 several features need to be explained. A luminescence intensity was the highest in the sample prepared (S1-1) or annealed (S1-2) at elevated temperature. This is mainly caused by an improvement in crystallinity, increase in doping efficiency, and increase of particle size. The as prepared nanoparticles (S1-3, S1-4 and S1-5) exhibited low luminescent efficiency arising from grain boundary effects. Namely, the activator ion in the crystal is most efficient when located in the bulk in a regular crystal field; activator ions located on the surface or on the grain boundaries are considered to be non-luminescent or even luminescence quenching regions. Clearly, these effects are more prominent in smaller nanoparticles due to their high surface areas.

Unlike $\text{GdVO}_4:\text{Dy}^{3+}$ where both excited VO_4^{3-} and Gd^{3+} ions may transfer energy to dopant Dy^{3+} ions, in the case of undoped DyVO_4 energy transfer to Dy^{3+} ions is possible only from VO_4^{3-} . This could explain the lower luminescence intensity in the samples of Series 2. In fact, a significant luminescence intensity was observed only in the sample prepared at elevated temperature (S2-1), almost certainly due to the above-mentioned effects.

3.2.3. Photoluminescence emission spectra in the NIR spectral region and photoluminescence excitation spectra

In the NIR region from 1100 nm to 1450 nm, similar PL spectra were recorded for both the bulk $\text{GdVO}_4:\text{Dy}^{3+}$ (sample S1-1, Fig. 7) and the bulk DyVO_4 (sample S2-1, not reported here) using excitation wavelengths 330 nm (Xenon lamp) and 488 nm (argon line). Several bands centered at $\lambda = 1178, 1294$, and 1371 nm and respectively attributed to the f–f transitions $^4\text{F}_{9/2} \rightarrow ^6\text{F}_{5/2}$, $^6\text{F}_{11/2} + ^6\text{H}_{9/2} \rightarrow ^6\text{H}_{15/2}$, and $^4\text{F}_{9/2} \rightarrow ^6\text{F}_{1/2}$ were observed [28]. However, a weak emission signal in the NIR region was found for all other samples of both series. Moisture adsorbed on nanoparticle surfaces

is likely responsible for quenching of luminescence. Note that the first band (Fig. 7) contains several sharp lines at: 1131 nm, 1148 nm, 1161 nm, 1178 nm and 1196 nm and it resembles emission in the Vis region around 580 nm. This could be seen as the emission of the second order [29].

In order to estimate the most suitable pumping scheme for the emission bands at 1178 nm and 1371 nm, excitation measurements were performed on the bulk systems (the sample S1-1) and excitation spectra divided by lamp spectrum are given on Fig. 8.

By analyzing the excitation spectra shown in Fig. 8, it is possible to conclude that the $\text{VO}_4^{3-} \rightarrow \text{Dy}^{3+}$ energy transfer is very efficient and that absorption coefficient of the vanadate charge-transfer transition is several orders of magnitude higher than that of the 4f transitions in the Dy^{3+} ions.

Finally, the following value for quantum yield at 330 nm was obtained by quantum yield measurements of $\text{GdVO}_4:\text{Dy}^{3+}$: 6.5% (bulk material), 5.4% (nanoparticles of 20 nm) and 0.1% (nanoparticles of 2 nm). For the sake of comparison, quantum yields for 2 at. % Dy^{3+} doped GdVO_4 samples annealed at 500 and 900 °C were found to be 4% and 7%, respectively [30]. However, note that the maximum value of quantum yield of 26.3% was determined for the bulk sample at 310 nm. Extremely high quantum efficiency could be assigned to charge transfer attributed to the VO_4^{3-} groups.

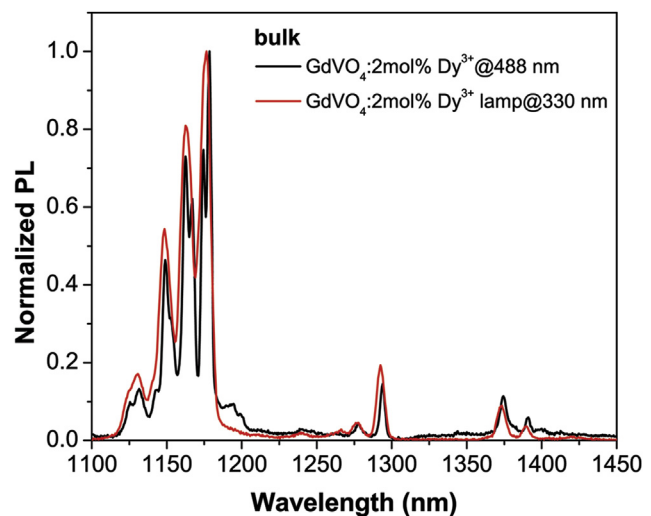


Fig. 7. NIR PL spectra (from 1.10 to 1.45 μm) of the bulk $\text{GdVO}_4:\text{Dy}^{3+}$ (sample S1-1) under (lamp) 330 nm and (laser) 488 nm excitation.

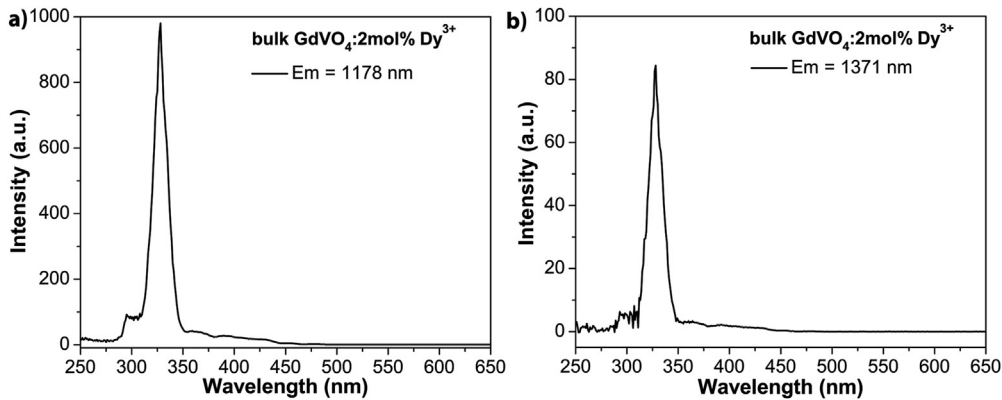


Fig. 8. Excitation spectra of the bulk $\text{GdVO}_4:\text{Dy}^{3+}$ (sample S1-1) monitoring the emission at 1178 nm and at 1371 nm.

4. Conclusions

$\text{GdVO}_4:\text{Dy}^{3+}$ and DyVO_4 samples with particles of different morphology and size were prepared by four synthetic methods: spherical nanoparticles of 2 nm, 4 nm, and 20 nm in size, nanorods with a few nanometers in diameter and up to 10–20 nm in length and microparticles of 1–8 μm (bulk material). XRD measurements evidenced that all GdVO_4 particles crystallized in a single tetragonal zircon-type crystal structure with space group $I4_1/\text{amd}$ indicating that the dopant Dy^{3+} ions are successfully incorporated into the host lattice, due to equal valence and similar ionic radii between Dy^{3+} and Gd^{3+} ions. Micro-Raman measurements support the XRD measurements. For the bulk materials, the difference in the Raman position was observed and it could be attributed to the different atomic number of Dy and Gd. Analyzing the emission spectra, in the UV–Vis spectral region, all the spectra show the Dy^{3+} ions emission from two closely separated states (${}^4\text{F}_{9/2}$ and ${}^4\text{I}_{15/2}$) to the ground state (${}^6\text{H}_{15/2}$), peaking at 483 and 455 nm, and from ${}^4\text{F}_{9/2}$ to the ${}^6\text{H}_{13/2}$ transition peaking at 572 nm, while emission spectra in the NIR spectral region exhibit several bands at $\lambda = 1178$, 1294, 1371 nm, which are attributed to ${}^4\text{F}_{9/2} \rightarrow {}^6\text{F}_{5/2}$, ${}^6\text{F}_{11/2} + {}^6\text{H}_{9/2} \rightarrow {}^6\text{H}_{15/2}$, ${}^4\text{F}_{9/2} \rightarrow {}^6\text{F}_{1/2}$ transitions, respectively. Due to strong emission in the NIR spectral region, these luminescent $\text{GdVO}_4:\text{Dy}^{3+}$ and DyVO_4 (bulk) particles incorporated in silica waveguides could find potential application for enhancement of 1.3 μm photoluminescence.

Acknowledgments

Part of this research was done during visit of D.J. to IFN-CNR CSMFO Lab. and FBK Photonics Unit, Povo-Trento, Italy, in the framework of the STSM (Grant No. 38223) from the project: COST Action MP 1401 “Advanced Fibre Laser and Coherent Source as tools for Society, Manufacturing and Lifescience” (2014–2018). The authors from Vinča Institute of Nuclear Sciences acknowledge the financial support of the Ministry of Education, Science and Technological Development of the Republic of Serbia (Project No: 45020 and 172056). L.T.N. Tran acknowledges the scholarship of the Ministry of Education and Training, Vietnam International Education Development. T. G. acknowledges the ERDF PostDoc project No. 1.1.1.2/VIAA/1/16/215 (1.1.1.2/16/I/001).

References

- [1] W.M. Yen, S. Shionoya, H. Yamamoto, *Practical Applications of Phosphors*, CRC Press, Michigan, 2006.
- [2] X. Chen, Y. Liu, D. Tu, *Lanthanide-doped Luminescent Nanomaterials: from Fundamentals to Bioapplications*, Springer, New York, 2014.
- [3] P.C. de Sousa Filho, T. Gacoin, J.-P. Boilot, R.I. Walton, O.A. Serra, Synthesis and luminescent properties of $\text{REVO}_4-\text{REPO}_4$ ($\text{RE} = \text{Y}, \text{Eu}, \text{Gd}, \text{Er}, \text{Tm}$, or Yb) heteronanostructures: a promising class of phosphors for excitation from NIR to VUV, *J. Phys. Chem. C* 119 (2015) 24062–24074.
- [4] T. Kim, N. Lee, Y. Park, J. Kim, J. Kim, E.Y. Lee, M. Yi, B.-G. Kim, T. Hyeon, T. Yu, H.B. Na, Mesoporous silica-coated luminescent Eu^{3+} doped GdVO_4 nanoparticles for multimodal imaging and drug delivery, *RSC Adv.* 4 (2014) 45687.
- [5] Z. Xu, C. Li, Z. Hou, J. Lin, Morphological control and luminescence properties of lanthanide orthovanadate LnVO_4 ($\text{Ln} = \text{La to Lu}$) nano-/microcrystals via hydrothermal process, *CrystEngComm* 13 (2011) 474–482.
- [6] M. Yi, S. Park, C. Seong, Y. Piao, T. Yu, The general synthesis and characterization of rare earth orthovanadate nanocrystals and their electrochemical applications, *J. Alloy. Comp.* 693 (2016) 825–831.
- [7] Z. Antić, M.D. Dramićanin, K. Prashanthi, D. Jovanović, S. Kuzman, T. Thundat, Pulsed laser deposited dysprosium-doped gadolinium-vanadate thin films for noncontact, self-referencing luminescence thermometry, *Adv. Mater.* 28 (2016) 7745–7752.
- [8] T.V. Gavrilović, D.J. Jovanović, V. Lojpur, M.D. Dramićanin, Multifunctional Eu^{3+} - and $\text{Er}^{3+}/\text{Yb}^{3+}$ -doped GdVO_4 nanoparticles synthesized by reverse micelle method, *Sci. Rep.* 4 (2014) 4209–4217.
- [9] S. Comby and J.-C. G. Bünzli, Lanthanide near-infrared luminescence in molecular probes and devices, in *Handbook on the Physics and Chemistry of Rare Earths*, Elsevier B. V., Amsterdam, vol. 37, Ch 235.
- [10] Y. Dwivedi, S.B. Rai, Spectroscopic study of Dy^{3+} and $\text{Dy}^{3+}/\text{Yb}^{3+}$ ions co-doped in barium fluoroborate glass, *Opt. Mater.* 31 (2009) 1472–1477.
- [11] L. Marciñak, K. Prorok, A. Bednarkiewicz, Size dependent sensitivity of $\text{Yb}^{3+}, \text{Er}^{3+}$ upconverting luminescent nano-thermometers, *J. Mater. Chem. C* 5 (2017) 7890–7897.
- [12] T. Gavrilović, J. Periša, J. Papan, K. Vuković, K. Smits, D.J. Jovanović, M.D. Dramićanin, Particle size effects on the structure and emission of $\text{Eu}^{3+}: \text{LaPO}_4$ and EuPO_4 phosphors, *J. Lumin.* 195 (2018) 420–429.
- [13] H. Li, X. Pu, J. Yin, X. Wang, S. Yao, H.M. Noh, J.H. Jeong, Effect of crystallite size and crystallinity on photoluminescence properties and energy transfer of $\text{Y}_6\text{MoO}_{12}:\text{Eu}$, *J. Am. Ceram. Soc.* 99 (2016) 954–961.
- [14] M. Vosoughifar, Dysprosium vanadate nanoparticles: morphology-controlled preparation, characterization and investigation of photocatalytic properties, *J. Mater. Sci. Mater. Electron.* 28 (2017) 13976–13982.
- [15] V. Muhr, M. Buchnera, T. Hirsch, D.J. Jovanović, S.D. Dolić, M.D. Dramićanin, O.S. Wolfbeis, Europium-doped GdVO_4 nanocrystals as a luminescent probe for hydrogen peroxide and for enzymatic sensing of glucose, *Sensor. Actuator. B* 241 (2017) 349–356.
- [16] T.V. Gavrilović, D.J. Jovanović, K. Smits, M.D. Dramićanin, Multicolor upconversion luminescence of $\text{GdVO}_4:\text{Ln}^{3+}/\text{Yb}^{3+}$ ($\text{Ln}^{3+} = \text{Ho}^{3+}, \text{Er}^{3+}, \text{Tm}^{3+}, \text{Ho}^{3+}/\text{Er}^{3+}/\text{Tm}^{3+}$) nanorods, *Dyes Pigments* 126 (2016) 1–7.
- [17] T.V. Gavrilović, D.J. Jovanović, L.V. Trandafilović, M.D. Dramićanin, Effects of Ho^{3+} and Yb^{3+} doping concentrations and Li^{+} co-doping on the luminescence of GdVO_4 powders, *Opt. Mater.* 45 (2015) 76–81.
- [18] L. Yang, L. Li, M. Zhao, G. Li, Size-induced variations in bulk/surface structures and their impact on photoluminescence properties of $\text{GdVO}_4:\text{Eu}^{3+}$ nanoparticles, *Phys. Chem. Chem. Phys.* 14 (2012) 9956–9965.
- [19] P.P. Rodenbough, C. Zheng, Y. Liu, C. Hui, Y. Xia, Z. Ran, Y. Hu, S.-W. Chan, Lattice expansion in metal oxide nanoparticles: MgO , Co_3O_4 , and Fe_2O_4 , *J. Am. Ceram. Soc.* 100 (2017) 384–392.
- [20] I. Guedes, Y. Hirano, M. Grimsditch, N. Wakabayashi, C.-K. Loong, Raman study of phonon modes in ErVO_4 single crystals, *J. Appl. Phys.* 90 (2001) 1843–1846.
- [21] C.C. Santos, E.N. Silva, A.P. Ayala, I. Guedes, P.S. Pizani, C.-K. Loong, L.A. Boatner, Raman investigations of rare earth orthovanadates, *J. Appl. Phys.* 101 (2007), 053511–1–053511–5.
- [22] G. Gouade, P. Coloban, Raman Spectroscopy of nanomaterials: How spectra relate to disorder, particle size and mechanical properties, *Prog. Cryst. Growth Char. Mater.* 53 (2007) 1–56.

- [23] P. Haritha, I.R. Martin, K. Linganna, V. Monteseguro, P. Babu, S.F. Leon-Luis, C.K. Jayasankar, U.R. Rodriguez-Mendoza, V. Lavin, V. Venkatramu, Optimizing white light luminescence in Dy^{3+} -doped $Lu_3Ga_5O_{12}$ nano-garnets, *J. Appl. Phys.* 116 (2014), 174308.
- [24] Y. Pu, Y. Huang, T. Tsuboi, H. Cheng, H.J. Seo, Intrinsic $[VO_4]^{3-}$ emission of cesium vanadate $Cs_5V_3O_{10}$, *RSC Adv* 5 (2015) 73467–73473.
- [25] G. Mialon, S. Türkcan, A. Alexandrou, T. Gacoin, J.-P. Boillot, New insights into size effects in luminescent oxide nanocrystals, *J. Phys. Colloid Chem.* 113 (2009) 18699–18706.
- [26] S. Manjunatha, R.H. Krishna, T. Thomas, B.S. Panigrahi, M.S. Dharmaprkash, Moss-Burstein effect in stable, cubic $ZrO_2:Eu^{3+}$ nanophosphors derived from rapid microwave-assisted solution-combustion technique, *Mater. Res. Bull.* 98 (2018) 139–147.
- [27] N.S. Singh, R.S. Ningthoujam, G. Phaomei, S. Dorendrajit Singh, A. Vinu, R.K. Vatsa, Re-dispersion and film formation of $GdVO_4: Ln^{3+}$ ($Ln^{3+} = Dy^{3+}, Eu^{3+}, Sm^{3+}, Tm^{3+}$) nanoparticles: particle size and luminescence studies, *Dalton Trans.* 41 (2012) 4404–4412.
- [28] J. Feng, L. Zhou, S.-Y. Song, Z.-F. Li, W.-Q. Fan, L.-N. Sun, Y.-N. Yua, H.-J. Zhang, A study on the near-infrared luminescent properties of xerogel materials doped with dysprosium complexes, *Dalton Trans.* 7 (2009) 6593–6598.
- [29] D.K. Sardar, W.M. Bradley Raylon, M. Yowa, J.B. Gruber, B. Zandic, Optical transitions and absorption intensities of Dy^{3+} (4f⁹) in YSGG laser host, *J. Lumin.* 106 (2004) 195–203.
- [30] N. Shanta Singh, R.S. Ningthoujam, N. Yaiphaba, S. Dorendrajit Singh, R.K. Vatsa, Lifetime and quantum yield studies of Dy^{3+} doped $GdVO_4$ nanoparticles: concentration and annealing effect, *J. Appl. Phys.* 105 (2009) 064303–064307.